Studies on Horizontal Axis Wind Turbine with Passive Teetered Brake & Damper Mechanism*

Yukimaru SHIMIZU**, Yasunari KAMADA**
and Takao MAEDA**

In order to improve the reliability of megawatt wind turbines, the passive teetered brake & damper mechanism is applied. Its two unique effects, as its name implies, are braking and damping. The passive brake & damper mechanism is useful for variable speed control of the large wind turbine. It is comprised of teetering and feathering mechanisms. When the wind speed exceeds the rated wind speed, the blade is passively teetered in a downwind direction and, at the same time, a feathering mechanism, linked to the teetering mechanism through a connecting rod is activated. In this study, two kinds of blades, a twisted tapered blade and a non-twisted rectangular one, are used with this passive mechanism. Testing of the model horizontal axis wind turbine in a wind tunnel showed that the passive mechanism can suppress the over-rotational speed of the rotor. The velocity distribution around the rotating blade is measured by a two-dimensional laser Doppler velocity meter. It is found that the passive teetered brake & damper mechanism can suppress the over-rotational speed of the rotor, and the braking effect is caused by the reduction of the angle of inflow for the blade.

Key Words: Wind Mill, LDV, Velocity Distribution, Horizontal Axis Wind Turbine, Passive Teetered Brake & Damper Mechanism

1. Introduction

In recent years much progress has been made in the development of large wind turbines to produce electricity. Wind turbines with 1 MW output and a 60 m-diameter are being developed for the commercial market. One important aspect of these turbines is variable speed control.

This study describes (1) a new device for variable speed control, a passive teetered brake and damper mechanism whose purpose is output control of 1 MW-class wind turbines, and (2) the investigations of its performance. This new mechanism can make blades incline to downstream and also change the pitch by means of aerodynamic force acting on the blade. It suppresses the output power passively at the range of over rated power with two kinds of blade motion (over rotation is reduced). It has a damping effect on fluctuation force acting on the blade caused by gusts and the velocity difference between upper and lower areas in a rotating plane made by an atmospheric boundary layer.

This paper describes the experimental testing of the control performance of the output power for a model wind turbine with this mechanism in a wind tunnel. The velocity distributions around the blade are measured by a two-dimensional laser Doppler velocity meter, and a part of the relationships between that flow and the braking effect are described here. Furthermore, two kinds of blades, a twisted tapered blade and a non-twisted rectangular one, are used for this mechanism, and the effect is discussed.

2. Nomenclature

c : chord length [m]
Cp : power coefficient
Cp' : comparative power coefficient
D : drag force [N]
F : aerodynamic force [N]
H : peripheral force [N]
L : lift force [N]
M : moment around teetering axis [N·m]
n : rotational speed of the rotor [rpm]
P : output power [W]

* Received 13th July, 1997
** Department of Mechanical Engineering, Mie University, 1515 Kamihama-cho, Tsu-shi, Mie 514, Japan

r : radius [m]
R : rotor radius [m]
Q : torque [N·m]
U : wind speed [m/s]
u : axial velocity [m/s]
v : radial velocity [m/s]
W : relative velocity [m/s]
α : angle of attack [deg]
β : angle of inflow [deg]
γ : feathering angle [deg]
ζ : teetered angle [deg]
θ : setting pitch angle [deg]
λ : tip speed ratio
Ψ : azimuth angle [deg]

suffixes

F : fixed rotor
P : passive rotor

3. Experimental Apparatus and Methods

Figure 1 shows the schematic outline of the experimental equipment. The experiment is carried out in an open-jet wind tunnel with an outlet diameter of 1.6 m using a maximum wind speed of 15 m/s. The test wind turbine has three blades and a diameter of 1.4 m. The rotating plane is set at $1d$ (d : wind turbine diameter $\fallingdotseq$1.45 m) downstream from the wind tunnel outlet. The brake & damper mechanism is mounted in the boss. It is equipped with a torque meter, a variable speed generator, a potentio-meter for measuring azimuth angle, and a rotational speed sensor. A potentio-meter for measuring teetered angle is set in the hub. The rated wind speed of this wind turbine is about 11 m/s. Therefore, the operational performance of the passive mechanism is investigated in wind speeds ranging from 10 m/s to 12 m/s. The rotor speed (maximum 950 rpm) is controlled by the variable speed induction generator with a inverter generation system.

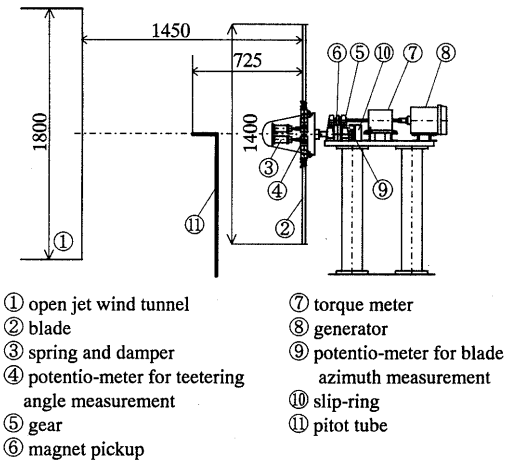

Fig. 1 Experimental apparatus

Table 1 shows the specifications for testing two kinds of blades, the twisted tapered blade and the non-twisted rectangular one.

Figure 2 shows the schematic outline of the passive teetered brake & damper mechanism. This mechanism is comprised of the blade holder on the teetering axis, the feathering lever connected to the blade axis, the rod end, the spring and damper. In the figure, the motion of the blade tip is shown by solid and broken lines. The root of the blade holder is restricted by the spring and damper. When aerodynamic force acts on the blade and the thrust force overcomes the spring force on the root, the blade inclines in the downstream direction. The blade axis, which is supported by the blade holder, can be rotated by the feathering lever and the rod end; that is, the feathering motion is controlled by the link mechanism. As a result, the teetering motion links the feathering motion around the blade axis. In this paper, the feathering motion means the variable pitch motion. The pitch is changed in the direction of increasing the angle of attack. Each blade is controlled independently by the brake and damper mechanism.

In the following discussion, a wind turbine rotor with the passive teetered brake & damper mechanism is called simply the passive rotor. A wind turbine rotor whose blades are fixed to a hub is called a fixed

Table 1 Configuration of test blades

	twisted and tapered blade	non-twisted and rectangular blade
airfoil section	NACA4415	NACA4412
tip chord length	143 mm	120 mm
root chord length	113 mm	120 mm
radius of rotor blade	700 mm	700 mm
twist angle	20 deg	-
aspect ratio	4.167	4.167

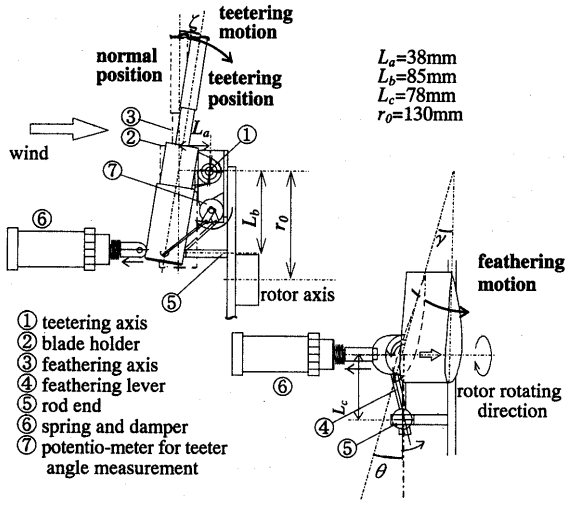

Fig. 2 Schematic outline of passive teetered brake & damper mechanism

rotor. The feathering angle is calculated geometrically by the relation of the teetered angle using the following equation:

$$\gamma=\tan^{-1}\left\{\frac{-L_a(1-\cos\zeta)+L_b\sin\zeta}{L_c}\right\} \quad (1)$$

L_a, L_b, and L_c are main dimensions of the mechanism shown in Fig. 2. The relationships between the teetered angle and the feathering angle is shown in Fig. 3.

The teetering motion caused by the aerodynamic force is controlled by a combination of the coil spring and damper. Measurements show the relationship between the moment, M, which acts on the blade and the teetered angle, ζ, to be as follows:

$$\zeta=0.941M-4.46 \quad (2)$$

In order to measure the velocity distribution around the rotating blades, a two-dimensional laser Doppler velocity meter (LDV) system is used. The laser is Argon ion with 4 W power and wavelengths of 514.5 nm for the green beam and 488.0 nm for the blue one. The focal length of this LDV system is 1.0 m with a beam expander. A probe is mounted on a traverse device. The axial and radial velocities are noted at each measuring position. The signals from the LDV probe are processed by the FVA signal processor and stored in a personal computer. In order to prevent any disturbance of the uniform flow, the tracer is poured from the inlet of the wind tunnel. The measuring positions in the axial and radial directions in the flow field are discussed in Sec. 4.3.

4. Experimental Results and Discussion

4.1 Performance comparison of the teetered brake & damper controlled hub (the passive rotor) and the fixed rotor

4.1.1 Relationships between the pitch angle and the power coefficient of both rotors Figure 4(a) shows the relationships between the power coefficient, Cp, and the tip speed ratio, λ. The graph described by the filled-in and blank symbols indicate the results of the passive rotor and the fixed rotor respectively. As the figure shows, the pitch angles represented by the symbols change in the range of -1 degree to $+2$ degree. The wind speed is set at 10 m/s. The measurement data are also compared with the results from Ref. (1)-(4) in the figure. In Fig. 4(a) the Cp_{max} for the passive rotor is 0.39 at $\lambda=3.5$ and that for the fixed rotor is 0.38 at $\lambda=3.6$. The Cp-λ curves depend a little on the pitch angle. However, the pitch angle, where the maximum of Cp_{max} is obtained, is 0 deg as shown in Fig. 4(b). Thus the experimental results at 0 deg are useful in the following discussion. The tip speed ratio for Cp_{max} is low (about 3.5), as shown in Fig. 4(a), because the thick blade with a small aspect ratio is used for the purpose of strengthening the blade in this experiment. Compared with the results obtained by I. K. Buehring[1], Cp is slightly higher in this experiment while the tip speed ratios at the point of Cp_{max} are almost the same. The results in the our previous paper with the blade aspect ratio of 5.714[2] and the results obtained by H. Munakata[3] have almost the same value for Cp_{max}, though the tip speed ratio at Cp_{max} is much larger ($\lambda=5-6$). In addition, the results of A. Yeznasni[4] in an experiment using a wind turbine included the tip speed ratio of 7-8 at Cp_{max}. As mentioned above, relationships between Cp and λ depend on various factors including the aspect ratio, planform, tip shape, and aerofoil of the blade. In the case of the wind tunnel tests, there is the limitation of outlet diameter, which places a size barrier on the aspect ratio of the blade.

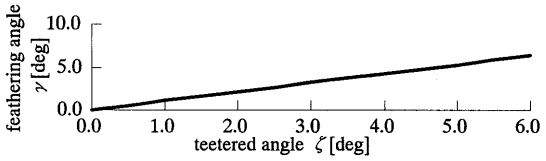

Fig. 3 Relationship between teetered angle, ζ, and feathering angle, γ

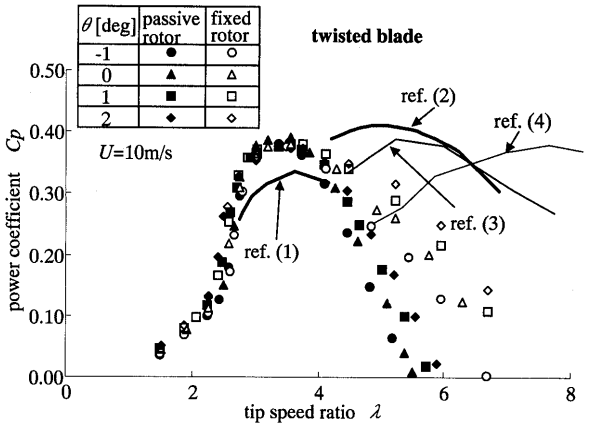

Fig. 4(a) Relationships between tip speed ratio, λ, and power coefficient, Cp (twisted blade)

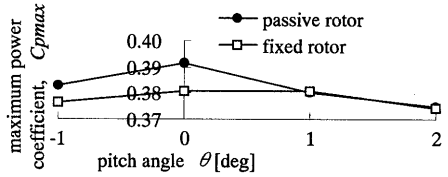

Fig. 4(b) Relationships between pitch angle, θ, and maximum power coefficient, Cp_{max} (twisted blade)

4.1.2 Comparison of performance of the passive rotor and the fixed rotor for various wind velocity Figure 5(a) shows the relationships between the output power, P, and the rotational speed of the rotor, n. The symbols and lines denote the passive and the

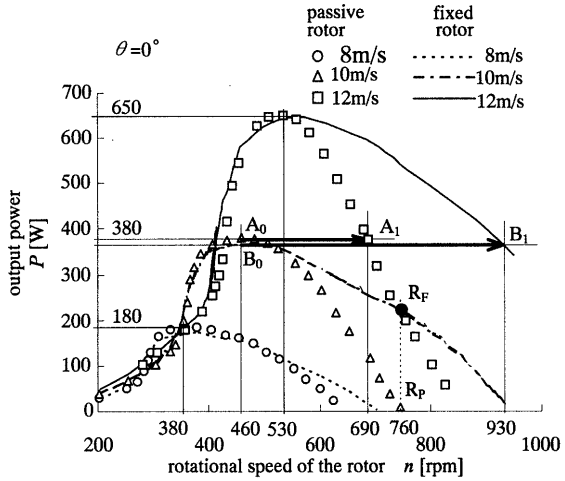

Fig. 5(a) Relationships between rotational speed of rotor, n, and output power, P (twisted blade)

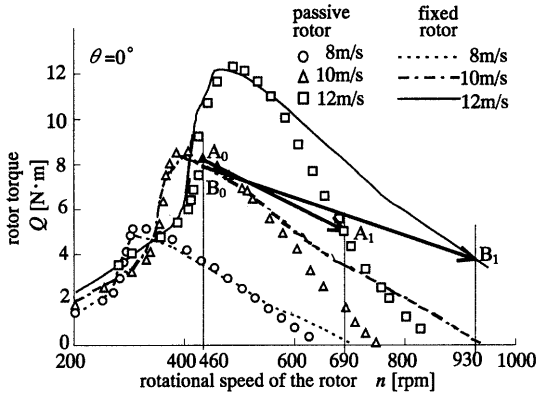

Fig. 5(b) Relationships between rotational speed of rotor, n, and torque, Q (twisted blade)

fixed rotors respectively. Figure 5(b) shows the relationships between the torque, Q, and the rotational speed of the rotor, n, for both rotors. The pitch angle is set at 0 deg and the wind speeds are fixed at 8, 10 and 12 m/s. The maximum output power for 8 m/s is 180 W at 380 rpm, or it is 380 W at 460 rpm for 10 m/s or it is 650 W at 530 rpm for 12 m/s. The rated wind speed is defined as 10 m/s in the experiment. In the case of the passive rotor (□ and △ symbols), the electric power is kept constant over the rated wind speed, 10 m/s, while the rotational speed of the rotor changes from 460 to 690 rpm, as indicated by A_0 to A_1 line in Fig. 5(a). In the case of the fixed rotor (solid and broken lines), the rotational speed is increased from 460 to 930 rpm, as indicated by B_0 to B_1 line. The results of constant power operation show that the passive teetered brake & damper mechanism can suppress the rotational speed from 930 rpm B_1 to 690 rpm A_1, a difference of 240 rpm. At the same time, the torque is reduced from A_0 to A_1 for the passive rotor, and from B_0 to B_1 for the fixed rotor.

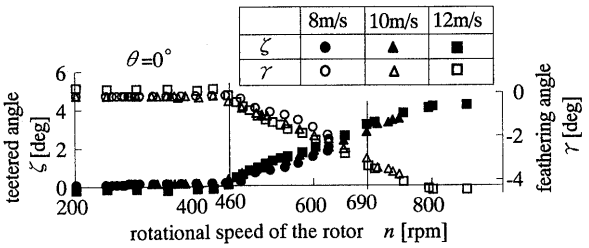

Fig. 5(c) Relationships among rotational speed of rotor, n, teetered angle, ζ, and feathering angle, γ (twisted blade)

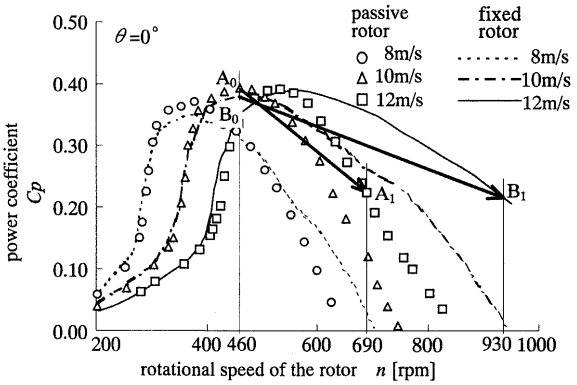

Fig. 5(d) Relationships between rotational speed of rotor, n, and power coefficient, Cp (twisted blade)

Figure 5(c) shows the relationships among the teetered angle, ζ, the feathering angle, γ, and the rotational speed of the rotor, n. The teetered angle is increased from 0.4 to 3.1 deg and the feathering angle is decreased from -0.4 to -3.3 deg, which is the reversible pitch control. Figure 5(d) shows the relationships between the power coefficient, Cp, and the rotational speed of the rotor, n. The Cp is changed from the point of maximum power, A_0, to that of lower power, A_1, for the passive rotor, and from B_0 to B_1 for the fixed rotor.

4.2 Comparisons of three kinds of performances of the passive controlled with the combination of the teetering and the feathering motions, the teeter controlled only, and the feather controlled only

Figure 6(a) shows the results of four kinds of output power curve using different controls. The symbols in the figure show refer to the fixed rotor, the teeter-control only, the feather-control only and the passive (combination of teeter and feather control).

Figure 6(b) shows the relationships between the rotational speed of the rotor, n, and the relative power coefficient Cp'. Cp' is the non-dimensional value of Cp divided by the baseline Cp of the fixed rotor at the same rotational speed. In Figs. 6(a) and (b) the

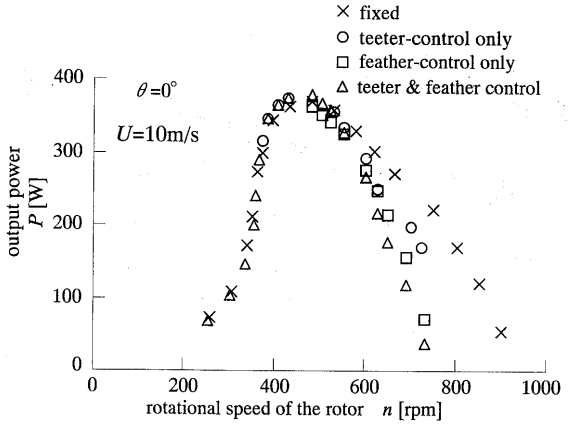

Fig. 6(a) Relationships between rotational speed of rotor, n, and output power, P with four kinds of control (twisted blade)

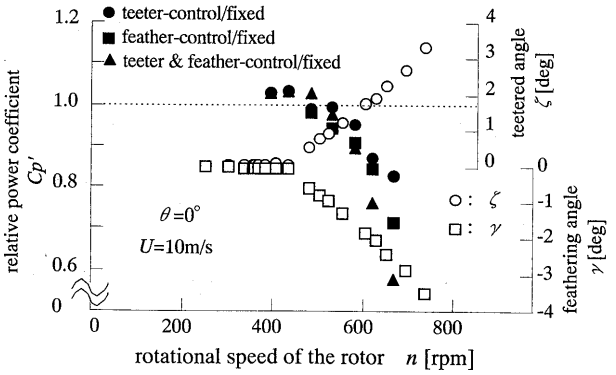

Fig. 6(b) Relationships between rotational speed of rotor, n, and relative power coefficient, Cp', with three types control (twisted blade)

pitch angle is set at 0 deg and the wind speed is fixed at 10 m/s. Comparisons at each control at a certain rotational speed of the rotor show some differences over the maximum Cp condition. In the operational condition where n is higher than that of Cp_{max}, the output power of the teeter-only or the feather-only control is lower than that of the fixed rotor, but higher than that of the passive control with a combination of the teeter and feather control. Therefore, the best results of suppression of power occur when the teetering and feathering motions are combined. In Fig. 6(b), Cp'(●, ■ and ▲)are larger than 1.0 near the point of the maximum output power(n=500 rpm). Such small variations of Cp' due to different controls are attributable to the initial setting of the pitch angle and also small defects in the manufacturing of the spring and damper.

4.3 The velocity distributions around the blade

Figure 7 shows a top view of measuring points around the blade. The flow velocity of each point is measured on a horizontal plane at the height of the rotor axis by the use of a two-dimensional LDV.

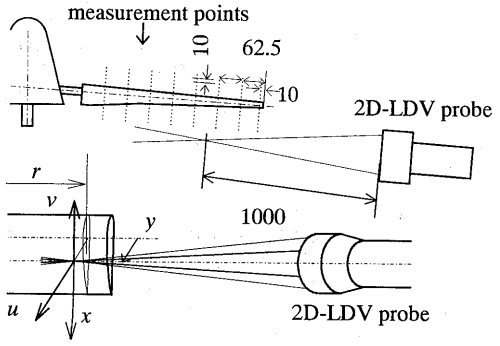

Fig. 7 LDV measuring points

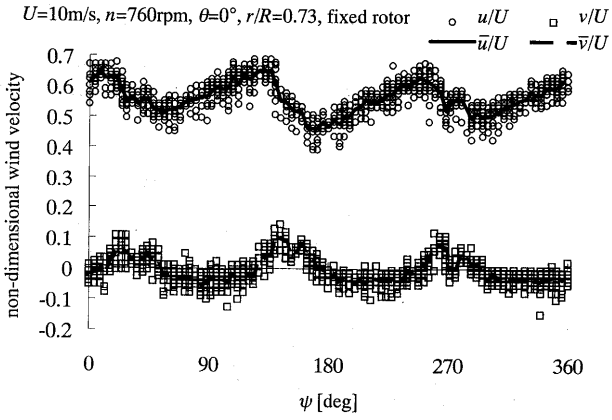

Fig. 8 Variation of velocity by the azimuth angle

Figure 8 shows the relationships between the azimuth angle, Ψ and the non-dimensional velocity. The measuring point is y/c=0.57 upstream from the rotor plane and r/R=0.73. The rotational speed of the rotor is 760 rpm in the non-load condition for the passive rotor. The symbols ○ and □ indicate the instantaneous velocity values, u/U for the axial component and v/U for the peripheral component respectively. Solid and broken lines indicate phase-lock averaged values of $\bar{u}/U$ and $\bar{v}/U$. The velocity data measured by the LDV are discontinuous, so that the phase-lock averaged values are used in following discussion. The instantaneous values have a scattering in 5% for the amplitude. However, the center of scattering is equal to the phase-lock averaged value, so that calculated value is useful for this experiment. When the blade is passing at the azimuth angles of Ψ=30, 150 and 270 deg, the axial velocity, $\bar{u}/U$, is increased as the blade approaches the measuring point, and then suddenly drops. The peripheral velocity, $\bar{v}/U$, shows the sharp edge hill at the blade passing at the azimuth angle of Ψ=30, 150 and 270 deg. It appears that there are some effects of a bound vortex on the blade.

Figures 9(a) and (b) show a velocity distribution around the rotating blade, which is measured at

the radius position of $r/R=0.73$ at 760 rpm. The passive rotor is operated in non-load condition at 760 rpm, which is pointed at R_P in Fig. 5(a). To make a comparison, the velocity distribution at 760 rpm is also selected for the fixed rotor, shown by R_F in Fig. 5(a). In Fig. 9(a), the velocity vectors in $x-y$ plane are drawn. As the blade cross-section moves to the left, a uniform wind flows in a downward direction in the figure. Figure 9(a) shows the velocity vectors on the stationary system. Each velocity vector is drawn at the relative position to the blade cross-section according to the blade azimuth angle. Figure 9(b) shows the relative velocity vector to the blade on the rotating system, which is the resultant vector of the blade rotating velocity and the flow velocity vector in Fig. 9(a). Figure 9(c) shows the schematic diagram of the lift forces, L_F, L_P, the drag forces, D_F, D_P and the peripheral forces, H_F, H_P at $r/R=0.73$, which is the typical radial position. The peripheral forces at the point of $r/R=0.73$ contribute much to generate the torque, and are considered under a two-dimensional flow condition. The power suppression for the passive rotor can be discussed from the point of view of the angle of inflow using the vectors shown in Fig. 9(b). The output power is assumed to be proportional to the torque because the rotational speeds of both rotors under consideration are the same, 760 rpm, which is achieved at non-load condition for the passive rotor. The torque is also proportional to forces H_F, H_P which contribute to rotation. In Fig. 9(c) α_F and α_P are the angles of attack, β_F and β_P are the angles of inflow, and W_F and W_P are the relative velocities on the blade coordinates. H_F and H_P are the peripheral components of both the resultant forces of the lift and drag. Therefore, using β_F and β_P, the following equations are obtained.

$$H_F=L_F\sin\beta_F-D_F\cos\beta_F\text{(Fixed rotor)} \quad (3)$$

$$H_P=L_P\sin\beta_P-D_P\cos\beta_P\text{(Passive rotor)} \quad (4)$$

As a result of the effect of passive control, the rotor blade inclines to $\zeta=3.7$[deg]in the downstream direction, while the relative velocities, W_F and W_P, are almost the same because the radial position changes little from r/R to $r/R\cos\zeta(=4$ deg). In Fig. 9(b) the angles of inflow(the typical point ① is assumed as the baseline angle of inflow)are identified and discussed below. Although the blade pitch of the passive rotor is changed to 3.8 deg in reverse pitch direction by the feathering motion, the angle of inflow becomes small, and the angle of attack becomes $\alpha_P=5.3$[deg]. In the figure, the angle of attack, $\alpha_P=5.3$[deg], is a little larger than $\alpha_F=3.8$[deg] for the fixed rotor. As a result, L_P and D_P are a little larger than L_F and D_F, respectively. Although the angle of inflow, β_P, is clearly smaller than β_F, and the direction of the resultant force F changes largely. Hence, the force, H_P which contributes to the rotation, is much lower than H_F. Furthermore, the radial position is reduced, and also the torque. It seems that the passive rotor is operated in non-load condition in this state. The torque of the fixed rotor at 760 rpm is large enough to accelerate the rotational speed and the fixed rotor is in non-load condition around 930 rpm.

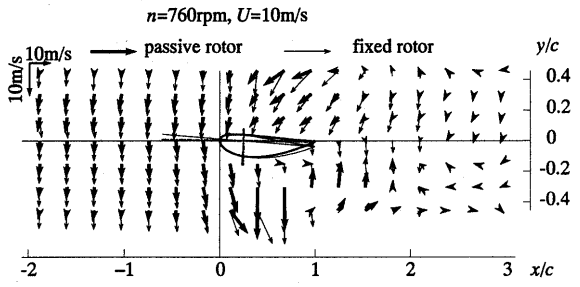

Fig. 9(a) Velocity vectors around rotating blade (Without rotating velocity, $n=760$ rpm)

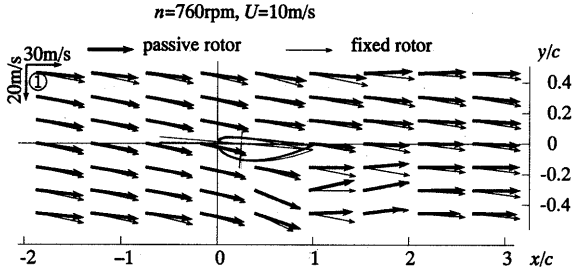

Fig. 9(b) Velocity vectors around rotating blade (Include rotating velocity, $n=760$ rpm)

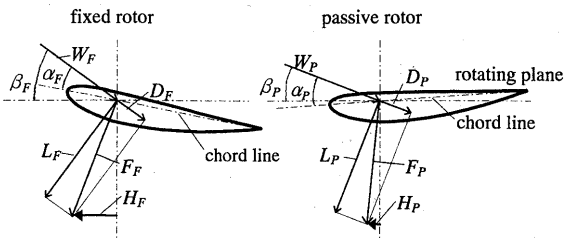

Fig. 9(c) Schematic diagram of the forces act on rotating blade at $r/R=0.73$

The interaction of the flow by all the blades will be presented in detail in the next paper. The discussion of the velocity vectors for Cp_{max} is omitted in this paper because the flow vectors for any control condition are almost the same.

4.4 Comparison of performances of the passive rotor with the twisted blades and that with the non-twisted blades

4.4.1 Relationships between the pitch angle and the power coefficient(with the non-twisted blade)

Figure 10 shows the relationships between the power coefficient, Cp, and the tip speed ratio, λ, of both

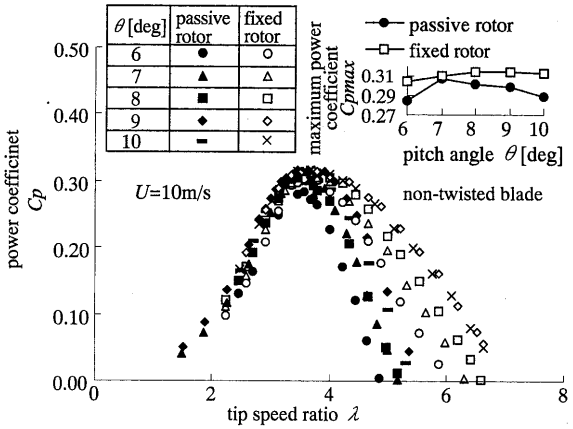

Fig. 10 Relationships between tip speed ratio, λ, and power coefficient, Cp (non-twisted blade)

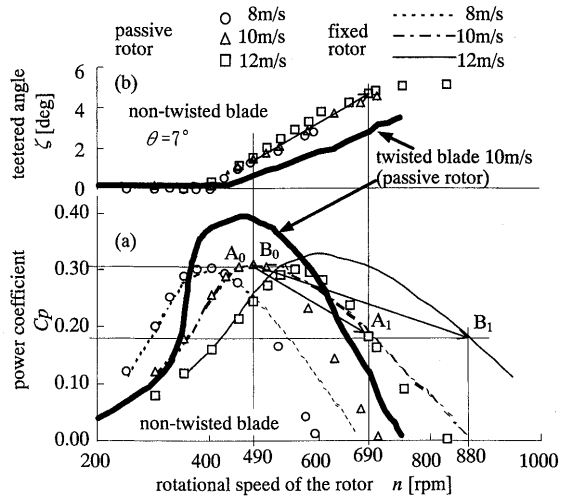

Fig. 11 Relationships among power coefficient, Cp, teetered angle, ζ and rotational speed of rotor, n (non-twisted blade)

rotors with the non-twisted blade shown in Table 1. The filled-in and blank symbols indicate the results of the passive and the fixed rotors respectively. Each symbol corresponds to a pitch angle, θ. The pitch angle is changed from 6 to 10 deg. The test wind speed is fixed at 10 m/s. In Fig. 10, the relationships between pitch angle, θ, and Cp_{max} are also indicated. The figure shows that the maximum value of Cp for each rotor is the same: $Cp_{max}=0.31$ at $\lambda=3.5$. However, when Cp_{max} is the largest, the pitch angle for each rotor is not the same: it is 7 deg for the passive rotor and 9 deg for the fixed rotor, since the passive rotor blades incline a little in the downstream direction at the Cp_{max} condition. There is small difference at Cp_{max} for both rotors. The relationship between Cp and λ is different for both rotors at various pitch angles. The pitch angle where Cp_{max} is the largest for the passive rotor is 7 deg. For the fixed rotor, Cp_{max} at a pitch angle of 7 deg is smaller than the Cp_{max} at 9 deg, while the difference is less than 0.01. The results that occurred at a pitch angle of 7 deg are presented in the following text.

4. 4. 2 Operational performance of the passive rotor and the fixed rotor for various wind velocities Figure 11 shows the relationships between the output power, P, and the rotational speed of the rotor, n. The symbols and lines show the results for the passive and the fixed rotors respectively. The pitch angle is set at 7 deg and the wind speeds are fixed at 8, 10 and 12 m/s, which are the same condition as that of Fig. 5(d). The operational performance will be discussed with the similar case of the twisted blade. In the case of the passive rotor, the electric power is kept constant over the rated wind speed, 10 m/s, while the rotational speed of the rotor changes from 490 to 690 rpm, as indicated by the A_0 to A_1 line in Fig. 11(a). By regulating the power in the manner described above, the rotational speed increases from 490 to 880 rpm for the fixed rotor, as indicated by the B_0 to B_1 line in Fig. 11(a). In constant power operation, the passive teetered brake & damper mechanism suppress the rotational speed by 190 rpm. The teetered angle is increased from 1.4 to 5.2 deg.

A comparison of the performances of the twisted and the non-twisted blades with the passive rotor shows both blades suppressing over-rotation in the range of over-rated wind speed. The performance curves at 10 m/s shows the rotational speed at Cp_{max} condition at 490 rpm with the non-twisted blade and 460 rpm with the twisted blade. The rotational speed of the non-twisted blade is higher than that of the twisted blade. But as Fig. 11(b) shows, the teetering motion of the non-twisted blade occurs at a rotational speed lower than that of the twisted blade. For the non-twisted blade the increasing rate of the teetered angle against the rotational speed is larger than that for the twisted blade; that is to say, the teetered angle at Cp_{max} condition with the twisted blade is small. The moment around the teetering axis caused by the thrust force for the non-twisted blade is larger than that for the twisted blade.

5. Conclusions

(1) The passive teetered brake & damper mechanism can suppress the over-rotational speed passively in the range over the rated wind speed.

(2) The power suppression of a rotor with the passive teetered brake & damper mechanism is carried out by the reduction of the peripheral component of the aerodynamic force caused by changing the angle of inflow.

(3) In the case of the twisted blade, the moment around the teetering axis is smaller than that of the

non-twisted blade. As a result, where the non-twisted blade concerned the teetering motion begins at a lower rotational speed when the same strength of spring are applied to two types of blades.

References

(1) Buehring, I. K. and Freris, L. L., Some aspects of small aerogenerator design and testing, Proc. Third Int. Symp. on WIND ENERGY SYSTEMS, Copenhagen, (1980), p. 297-305.

(2) Shimizu, Y., Matumura, S. and Imamura, H., Power Augmentation of Horizontal Axis Wind Turbine with Tip Vane(3rd Report, In Case of Taper Blade), Trans. Jpn. Soc, Mech. Eng., (in Japanese), Vol. 57, No. 543, B(1991), p. 205-210.

(3) Munakata, H., Kimura, S., Iuchi, M. and Abe, K., Wind Tunnel Test of Rotor Aerodynamics with Various Surface Roughness, Proc. 1990 Europ. Com. Wind Energy Conf., Madrid, (1990), p. 363-367.

(4) Yeznasni, A., Derdelinckx, R. and Hirsch, Ch., Influence of Dynamic Stall in the Aerodynamic Study of HAWT, Wind Energy: Technology and Implementation(Amsterdam EWEC '91), Amsterdam, (1991), p. 56-60.